Remote Sensing of Environment 229 (2019) 1–13

Contents lists available at ScienceDirect

Remote Sensing of Environment

journal homepage: www.elsevier.com/locate/rse

Hurricane damage detection on four major Caribbean islands

Kirsten M. de Beurs[a,*], Noel S. McThompson[a], Braden C. Owsley[a], Geoffrey M. Henebry[b,c]

[a] Department of Geography and Environmental Sustainability, University of Oklahoma, United States of America
[b] Department of Geography, Environment, and Spatial Sciences, Michigan State University, United States of America
[c] Center for Global Change and Earth Observations, Michigan State University, United States of America

ARTICLE INFO

Keywords:
Hurricanes
Droughts
MODIS
Disturbance
Tasseled Cap

ABSTRACT

Tropical cyclones are natural events that transform into natural disasters as they approach and reach land. In 2017 alone, tropical cyclones caused an estimated $215 billion in damage. While MODIS data are regularly used in the analysis of hurricanes and typhoons, damage studies typically focus on just a few events without providing a comprehensive overview and comparison across events. The MODIS record is now sufficiently long to enable standardization in time, allowing us to extend previously developed disturbance methodology and to remove dependency on land cover datasets. We apply this new approach to detect the impact of both droughts and hurricanes on the four largest Caribbean islands since 2001. We find that the percentage of disturbed land on the four islands varies from approximately 0–50% between 2001 and 2017, with the highest percentages coinciding with major droughts in Cuba, and Hurricane Maria in Puerto Rico. We demonstrate that (1) Hurricane Maria resulted in significant disturbance across 50% of Puerto Rico (4549 km^2), and (2) gradual recovery started about 2.5 months after the hurricane hit. While our approach focuses on the identification of damage arising from hurricanes, it is also capable of identifying the damage from droughts. This approach ultimately enables a better understanding of the combined effects of these two natural hazards across island landscapes.

1. Introduction

Tropical cyclones are natural events that transform into natural disasters as they approach and reach land. In 2017 alone, tropical cyclones caused an estimated US$215B in damage (Faust and Bove, 2017). Some have argued that increases in tropical sea surface temperature since the mid-1970s have increased the potential destructiveness of hurricanes as a result of longer storm lifetimes and greater storm intensities (Emanuel, 2005). However, there is still great uncertainty with respect to the effects of climate change on hurricane frequency and intensity (Lugo, 2000; Pielke Jr et al., 2005). For example, some of the latest climate projections forecast an increase in the intensity of tropical cyclones by 2–11%, while decreasing the frequency of the storms by 6–34% (Knutson et al., 2010).

Climate models also consistently predict drying for many low to mid-latitude regions, with drier areas predicted to get drier and wetter areas predicted to get wetter (Trenberth et al., 2014). In addition, as a result of increased temperatures, the rate of drying is expected to increase, resulting in the establishment of droughts more quickly and with greater intensity (Trenberth et al., 2014). It is not uncommon for ecosystems exposed to drought to also experience hurricanes (Beard et al., 2005; Ortegren and Maxwell, 2014). Both droughts and the excessive rainfall found during hurricanes have been linked to atmospheric circulation patterns, such as the Atlantic Multidecadal Oscillation (AMO; Curtis, 2008, Elder et al., 2014, Fensterer et al., 2012, Méndez and Magaña, 2010). The combined effect of these two natural events can be highly destructive, and actual hurricane recovery may take longer than expected following a major drought, such as was found for lakes (Xuan and Chang, 2014). Teasing apart the combined effect of even moderate hurricanes and moderate droughts is an important but complicated endeavor requiring a better understanding of ecosystem recovery processes following disturbance (Beard et al., 2005; Ortegren and Maxwell, 2014) and a standardized dataset that allows for the comparison of hurricane damage in a comprehensive manner.

Since 2001, 15 hurricanes have hit the Caribbean islands of Cuba, Hispaniola, Jamaica, and Puerto Rico, affecting the approximately 40 million people living on those islands (World Bank, 2018). Droughts have generally received less attention than other natural disasters in the Caribbean (Beard et al., 2005), but a new downscaled drought dataset demonstrated that between 2013 and 2016, the Caribbean faced its most severe and widespread drought since the 1950s (Herrera and Ault, 2017). This drought was especially significant during the summer of 2015, when in June drought conditions covered 95% of the four major islands in the Caribbean, with 82% under at least severe drought

* Corresponding author.
E-mail address: kdebeurs@ou.edu (K.M. de Beurs).

https://doi.org/10.1016/j.rse.2019.04.028
Received 18 September 2018; Received in revised form 6 March 2019; Accepted 26 April 2019

conditions and 58% under extreme drought. There are several global and a few regional drought datasets available for regions affected regularly by hurricanes, such as the Caribbean (Herrera and Ault, 2017). However, while remote sensing methods have been developed for the detection of hurricane damage over the past few years, especially focused on the detection of hurricane damage on forests (Negrón-Juárez et al., 2014), there are few long time series that allow for the standardized comparison of the effect of hurricanes.

The dense temporal resolution of MODIS data (daily, with 8-day composites) and the relatively long time series available (2000–current) make MODIS data ideally suited for the study of hurricane damage. MODIS data are indeed regularly used in the analysis of hurricane and typhoon damage (Chambers et al., 2007; Long et al., 2016; Parker et al., 2017; Rogan et al., 2011; Rossi et al., 2013); however, studies have typically focused on just one hurricane or, at best, a few and do not provide a comprehensive overview—an exception being Potter (2014). In addition, many of the MODIS analysis use simple vegetation indices such as the NDVI and the EVI, with few extending to indices such as the Tasseled Cap Water Index and the NDII (Jin and Sader, 2005; Wang and Xu, 2010). In contrast, Potter (2014) performed a more comprehensive analysis and presented a global assessment of damage to coastal ecosystem vegetation from tropical storms between 2006 and 2012 based on quarterly differences in vegetation index imagery. The Quarterly Indicator of Cover Change identified regions where at least a 40% change in green vegetation cover occurred, demonstrating that extensive tropical forest damage could be detected following extreme storm events (Potter, 2014). These data were not extended past 2012, and the relatively coarse spatial resolution used (5600 m) make them less than ideal for the study of the Caribbean islands.

We have previously shown that a MODIS-derived disturbance index based on standardized tasseled cap brightness, greenness, and wetness data as derived by Healey et al. (2005) can successfully detect forest clearance (de Beurs et al., 2016; Tran et al., 2016). We also demonstrated that the disturbance index can be adapted for use in grasslands (de Beurs et al., 2016). We have applied disturbance index analysis to the central United States to demonstrate that it is quite effective in identifying damage from tornados and can track the subsequent recovery phase (Kingfield and de Beurs, 2017).

A fundamental limitation of the disturbance index approach is that it is relative: it relies on a comparison of potentially damaged pixels against a normal distribution of typical “undamaged” pixels. For example, in the case of forest disturbance, the approach requires a large sample of normal, non-disturbed, forest pixels to serve as the baseline for comparison. As a result, the approach is highly dependent on a high-quality land cover map, and potentially information about aspect and slope (de Beurs et al., 2016). Yet, the quality of land cover datasets varies widely across the globe and low accuracies are prevalent, especially in areas with heterogeneous land cover (Gómez et al., 2016; Herold et al., 2008)

The MODIS record is now sufficiently long to enable standardization in time. Thus, here, we are extending the disturbance index approach by removing the dependency on a land cover dataset by using the length of the MODIS time series. We apply this new approach to detect the impacts of hurricanes since 2001 on the four largest Caribbean islands. By comparing the results against other standardized datasets, specifically developed for the detection of droughts, we demonstrate that it is also capable of identifying the impact of drought on the vegetated land surface.

2. Study region

We investigate the impact of hurricanes and droughts on the four largest islands in the Caribbean Sea: Cuba, Hispaniola (hosting Haiti and the Dominican Republic), Puerto Rico, and Jamaica. The total population across these four islands was nearly 40 million in 2016 (Table 1).

Table 1
Country population and GDP from the World Bank (2018).

Island	Country	Population	Total GDP (US$B)	*Per capita* GDP (US$)
Cuba	Cuba	11,475,982	80.656	7602
Hispaniola	Haiti	10,847,334	8.023	766
	Dominican Republic	10,649,791	71.584	7052
Puerto Rico	Puerto Rico	3,411,307	103.135	30,833
Jamaica	Jamaica	2,871,934	14.187	4879

Fig. 1 provides an overview map of the four islands based on the MODIS Land Cover data (MCD12Q1) with the Plant Functional Type (PFT) classification scheme from 2001. The most dominant land cover type was evergreen broadleaf forest for Jamaica (61%) and Puerto Rico (42%); whereas, it was broadleaf cropland for Cuba (46%) and grassland for Hispaniola (28%).

In the Atlantic Basin and Eastern Pacific, tropical cyclones with sustained wind speeds of > 118 kph and center pressure of 980 mbar are considered to be hurricanes. The Saffir-Simpson Hurricane Intensity Scale is used to further classify storms from Category 1 to Category 5. Each island has been hit by at least one hurricane since 2001, with Cuba enduring 11 hurricanes (Table 2).

3. Data

3.1. MODIS NBAR BRDF product – MCD43A4

We used the MODIS Nadir BRDF-Adjusted Reflectance Distribution Product (MCD43A4) version 6, which simulates surface reflectance values and is delivered daily, based on 16 days of observations (Schaaf et al., 2002), with 463 m spatial resolution. Both Terra and Aqua data are used in the generation of the product to increase the probability for a quality input to the models. We downloaded the data at eight-day intervals between 2001 and 2017 for four tiles: H10V06, H10V07, H11V06 and H11V07. For each of 782 time steps, we calculated the MODIS Tasseled Cap brightness, greenness, and wetness values (Lobser and Cohen, 2007) by multiplying each band coefficient by the corresponding band value and then summing these values for each index listed in Table 3.

After calculating these Tasseled Cap indices, we stacked the data in temporal order. Missing data were filled using a median filter centered on five sequential composites.

3.2. Hurricane paths

The Atlantic Hurricane Database (Atlantic HURDAT2, 2018; Landsea and Franklin, 2013) was downloaded from the National Hurricane Center (NHC), a division of the National Oceanographic and Atmospheric Administration (NOAA). Atlantic HURDAT2 provides the most accurate possible information on the track of historical hurricanes and tropical cyclones in the Atlantic Basin. HURDAT 2 provides six-hourly information on the location, maximum winds, and central pressure of all known tropical and subtropical cyclones from 1851 to 2016. Data for individual storms were also downloaded for Hurricanes Irma and Maria. These two storms fell outside of the Atlantic HURDAT2 database, but within the timeframe of the collected MODIS data. We only evaluated the data for cyclones occurring since January 1, 2001. We generated point files for the cyclone records, which we then intersected with the extent of the four major Caribbean islands to identify when (dates) and where (locations) the hurricane centers passed directly over land. These extracted point data for each event were converted to a line representing the track of the storm across the island.

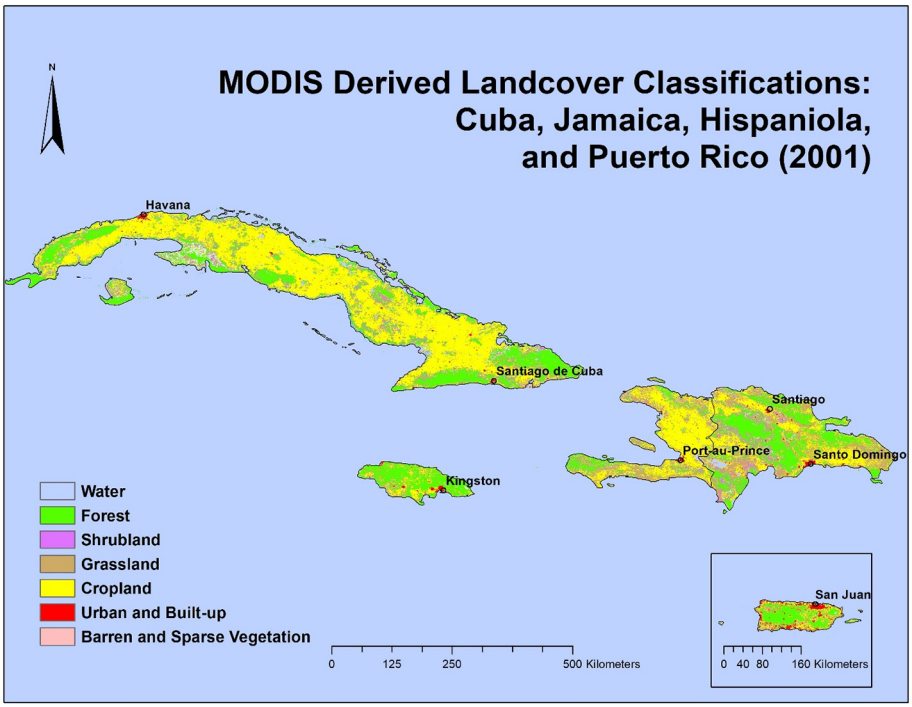

Fig. 1. Study region overview figure based on MODIS Land Cover data from 2001.

3.3. Drought data

The Caribbean has been affected by several severe droughts during our study period. To better understand the spatio-temporal landscape variability resulting from drought, we downloaded a high-resolution drought dataset statistically downscaled to 4 km spatial and monthly temporal resolution (Herrera and Ault, 2017). This dataset consists of self-calibrating Palmer Drought Severity Index data. For this study, we used all monthly observations between 2001 and 2016, which is the last year available in this dataset.

3.4. Validation data

To validate the disturbance index results, we downloaded high-resolution, optical satellite data from the Open Data Program provided by Digital Globe (https://www.digitalglobe.com/opendata). The Open Data Program provides high resolution, commercial satellite images for use in natural disaster damage identification. Of the 15 hurricanes that directly hit the islands, only data for Hurricane Matthew over Hispaniola and Hurricane Maria over Puerto Rico were available from the Open Data Program. For validation of Hurricane Matthew, we downloaded images from September 13, 2013 and October 15, 2016; for Hurricane Maria, we selected images from August 21, 2017 and October 16, 2017. These images were not entirely cloud-free, with cloud cover between 10% and 30%, but they provided the best opportunity for validation at high spatial resolution.

Table 3
MODIS Tasseled Cap Coefficients, from Lobser and Cohen (2007).

Band	Brightness	Greenness	Wetness
Red	0.4395	−0.4064	0.1147
NIR 1	0.5945	0.5129	0.2489
Blue	0.2460	−0.2744	0.2408
Green	0.3918	−0.2893	0.3132
NIR 2	0.3506	0.4882	−0.3122
SWIR 1	0.2136	−0.0036	−0.6416
SWIR 2	0.2678	−0.4169	−0.5087

Table 2
Named hurricanes with maximum windspeeds in kilometers/h (miles/h). Some hurricanes lasted multiple days.

Hurricane	Category	Max Wind Speed (km/h)	Max Wind Speed (miles/h)	Date	Island
Michelle	3	185	115	11/04/01	Cuba
Isidore	1	121	75	09/20/02	Cuba
Lili	1	145	90	10/01/02	Cuba
Charley	2	169	105	08/13/04	Cuba
Dennis	3	193	120	07/08/05	Cuba
Gustav	3	193	120	08/31/08	Cuba
Ike	3	185	115	09/08/08	Cuba
Paloma	1	145	90	11/09/08	Cuba
Sandy	1	121	75	10/24/12	Jamaica
Sandy	2	161	100	10/25/12	Cuba
Matthew	3	209	130	10/04/16	Hispaniola
Matthew	3	185	115	10/05/16	Cuba
Irma	5	266	165	09/09/17	Cuba
Maria	4	249	155	09/20/17	Puerto Rico
Maria	3	201	125	09/22/17	Hispaniola

4. Methods

4.1. MODIS disturbance index with temporal standardization

Following methodology described previously in other papers, we standardized the TC brightness, greenness, and wetness before combining these into a Disturbance Index (DI) (de Beurs et al., 2016; Healey et al., 2005; Tran et al., 2016). The normalization was carried out as follows:

$$Brightness_n(t) = (Brightness(t) - \mu Brightness)/\sigma Brightness \quad (1)$$

$$Greenness_n(t) = (Greenness(t) - \mu Greenness)/\sigma Greenness \quad (2)$$

$$Wetness_n(t) = (Wetness(t) - \mu Wetness)/\sigma Wetness \quad (3)$$

where t is a composite at time t and μ and σ are the mean and the standard deviation, respectively, of the particular index for that composite over the years. In previous papers, the mean and standard deviation calculations were carried out spatially, where each pixel was compared to a distribution of values extracted from pixels with the same land cover. The disadvantage of this approach is that it is highly dependent on high quality land cover classification. In addition, aspect and slope can have a strong influence on pixels even within the same land cover (de Beurs et al., 2016). The MODIS time series now extends 17 full years (2001–2017). As a result, there are a sufficient number of observations to enable the development of normal distributions of values in time. Thus, in Eqs. (1) to (3), the mean and the standard deviations were calculated based on the anniversary composites from every year. In other words, the first pixel in the first composite in the first year is compared to the mean and the standard deviation of the first pixel for all first composites of each year. Thus, January 1, 2001 is compared with the mean and the standard deviation of all January 1 composites between 2001 and 2017.

When natural vegetation is damaged as the result of a hurricane or tornado (Kingfield and de Beurs, 2017), greenness and wetness typically decline as a result of vegetation loss while brightness increases, because damaged areas typically absorb less solar radiation than areas with healthy vegetation. As a result, we can calculate the disturbance index as follows:

$$DI(t) = Brightness_n(t) - (Greenness_n(t) + Wetness_n(t)) \quad (4)$$

Since normalized distributions typically have a mean of 0 and a standard deviation of 1, we expect high DI values when there is a lot of disturbance. For example, if a pixel brightness value is two standard deviations brighter than average, *i.e.*, its normalized value is 2, and the greenness and wetness are two standard deviations less than average, *i.e.*, their normalized values are −2, then the resulting DI value is 6 (=2 − (−2 + −2)).

When normalized distributions are added or subtracted, their mean and standard deviations are added (they are never subtracted). In de Beurs et al. (2016), we demonstrated that if we set the threshold of disturbance at 3, we have a 15.9% probability of identifying a pixel as disturbed when, in fact, it is not (*i.e.*, a false positive). Here we will identify disturbed areas both based on a threshold of 2 (probability of false positive equals 25.2%) and a threshold of 3. Note that the probability of a false positive is 9.1% for a disturbance value of 4, and 4.8% for a disturbance value of 5.

4.2. Testing for normality

To compare composites properly, we need to assess whether the sampling distribution of pixels follows a normal distribution. Several tests have been developed to test for normality. For all those tests, the null hypothesis is the "sample distribution is normal"; thus, a significant result indicates that the sampling distribution may deviate from normality. One drawback of normality tests is their low power for small sample sizes (Steinskog et al., 2007). Here we applied the Shapiro-Wilk test to test for normality. The Shapiro-Wilk test is based on the correlation between our observations and corresponding normal scores, and it can be used for very small sample sizes. In addition, for small sample sizes, this test provides better power than the Kolmogorov-Smirnov test (Steinskog et al., 2007). We carried out the test for normality for each of the 46 composites, evaluating the anniversary composites over the 17-year period.

4.3. Validation

Before and after images provided by the Open Data Program for Hurricane Matthew were overlaid to establish the overlapping area. We randomly selected 25 independent validation regions consisting of four MODIS pixels each. Each validation region was visually inspected to determine the dominant land cover type and to determine the presence of identifiable hurricane damage. For the samples that visually presented hurricane damage, we identified the disturbance index values based on the MODIS data both before the hurricane hit and three weeks after the hurricane went through. The same process was completed using the Hurricane Maria images over Puerto Rico. We randomly selected 46 independent validation regions consisting of four MODIS pixels each for Hurricane Maria. We were able to select more validation points in Puerto Rico, because the overall area with hurricane damage was larger with a greater diversity in land cover types. Note that in this validation, we focus specifically on the ability of the disturbance data to quantify disturbance. As a result, the validation focuses on areas with hurricane damage and we have not carried out a specific validation for areas without damage. Nevertheless, we do confirm that the disturbance index is close to zero (the expected value for no damage) before the hurricanes hit.

5. Results

5.1. MODIS DI and standardization results

Fig. 2 provides the mean brightness, greenness, and wetness images for Cuba. With brightness values displayed in red, greenness values displayed in green, and wetness values displayed in blue, the map of the mean values of the Tasseled Cap Indices closely resembles the MODIS derived land cover data. Urban areas have higher values in the brightness index, but lower values in wetness and greenness. These areas show up in orange and red colors. Forests present higher values in greenness, moderate values in wetness, and lower values in brightness. As a result, forest areas show up in darker green colors. Water has virtually no brightness or greenness and, thus, appears blue. Croplands and grasslands appear in mixtures from brown to yellows.

We applied the Shapiro-Wilk test to determine the number of composites that do not follow a normal distribution in brightness, greenness, and wetness data separately and found that 99.9% of all pixels exhibited normality for > 90% of all composites. As a result, we concluded that our standardization method based on the normal distribution generates valid observations.

5.2. Disturbance detection: droughts

The percentage of disturbed land on the four islands varies from approximately 0–50%, with the highest percentages coinciding with major droughts (Fig. 3) and immediately after hurricane Maria in Puerto Rico (Fig. 6).

It is apparent that longer periods of drought result in greater overall disturbance and that rainfall quickly alleviates drought effects, *e.g.*, in Cuba there was a major drought through 2004 and early 2005, ending later that year. The percentage of disturbed pixels increased almost immediately at the beginning of the drought and remained high throughout the period. By 2005, 45% of Cuba (49,446 km^2) was

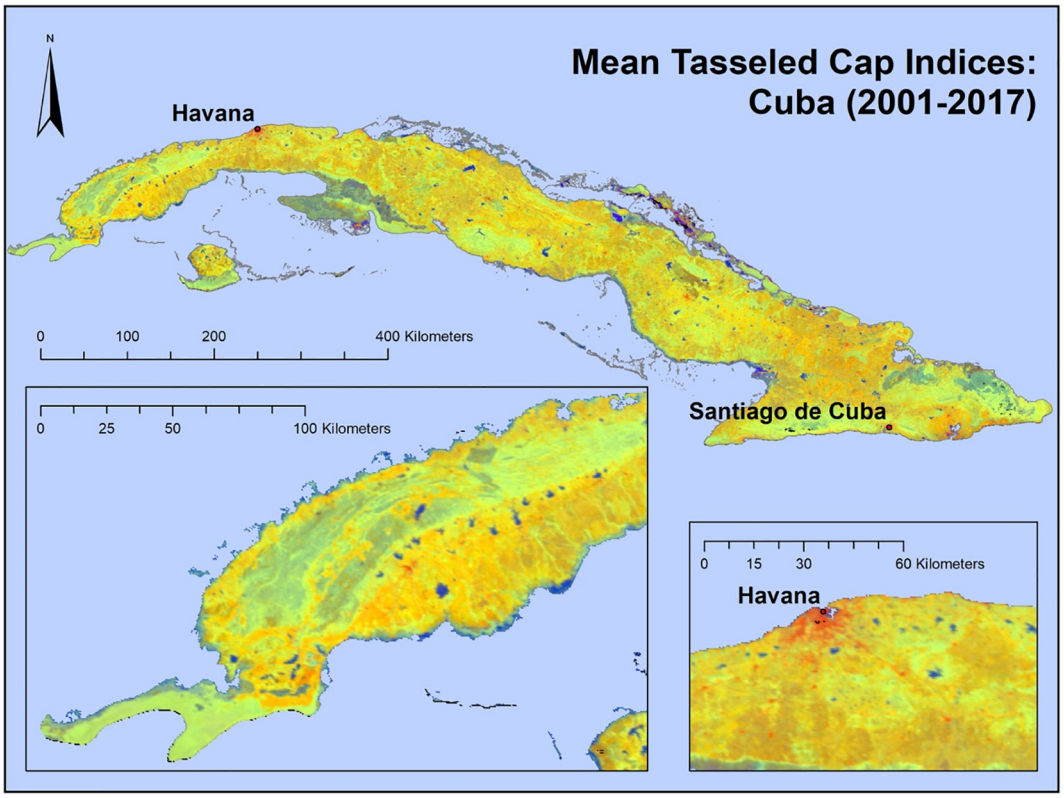

Fig. 2. Three colour composite of the mean Brightness, Wetness, and Greenness Tasseled Cap Indices for the island of Cuba. Lower left inset showing forests on the eastern end of the island. Lower right inset showing Havana and surrounding area.

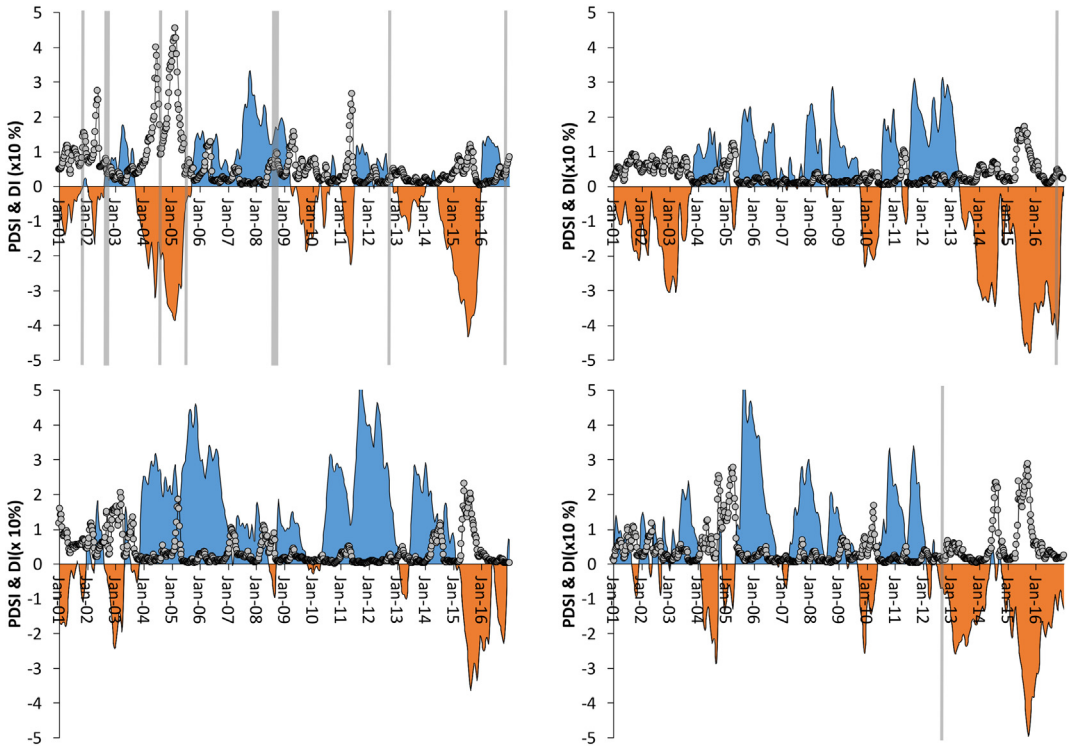

Fig. 3. Orange and blue provide the Palmer Drought Severity Index for Cuba (upper left), Hispaniola (upper right), Puerto Rico (lower left), and Jamaica (lower right). The dotted line provides the percentage (divided by 10 for visualization) of the island that is classified as disturbed (DI > 3). Large drought periods are linked with strong disturbances, for example the 2004/2005 drought in Cuba disturbed 45% of the island. The vertical lines indicate the timing of the hurricanes; in the case of two hurricanes within one month only one vertical line is drawn. (For interpretation of the references to colour in this figure legend, the reader is referred to the web version of this article.)

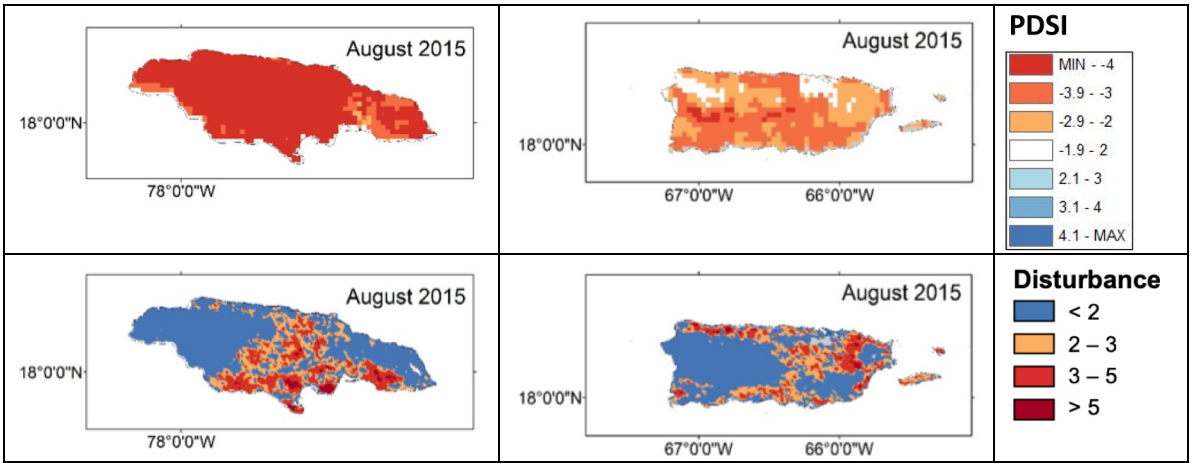

Fig. 4. Maximum drought months (upper pair) on Jamaica (left) and Puerto Rico (right) with the corresponding disturbance index data (lower pair) for that month. Severe droughts have negative PDSI values and disturbed land has values over 2.

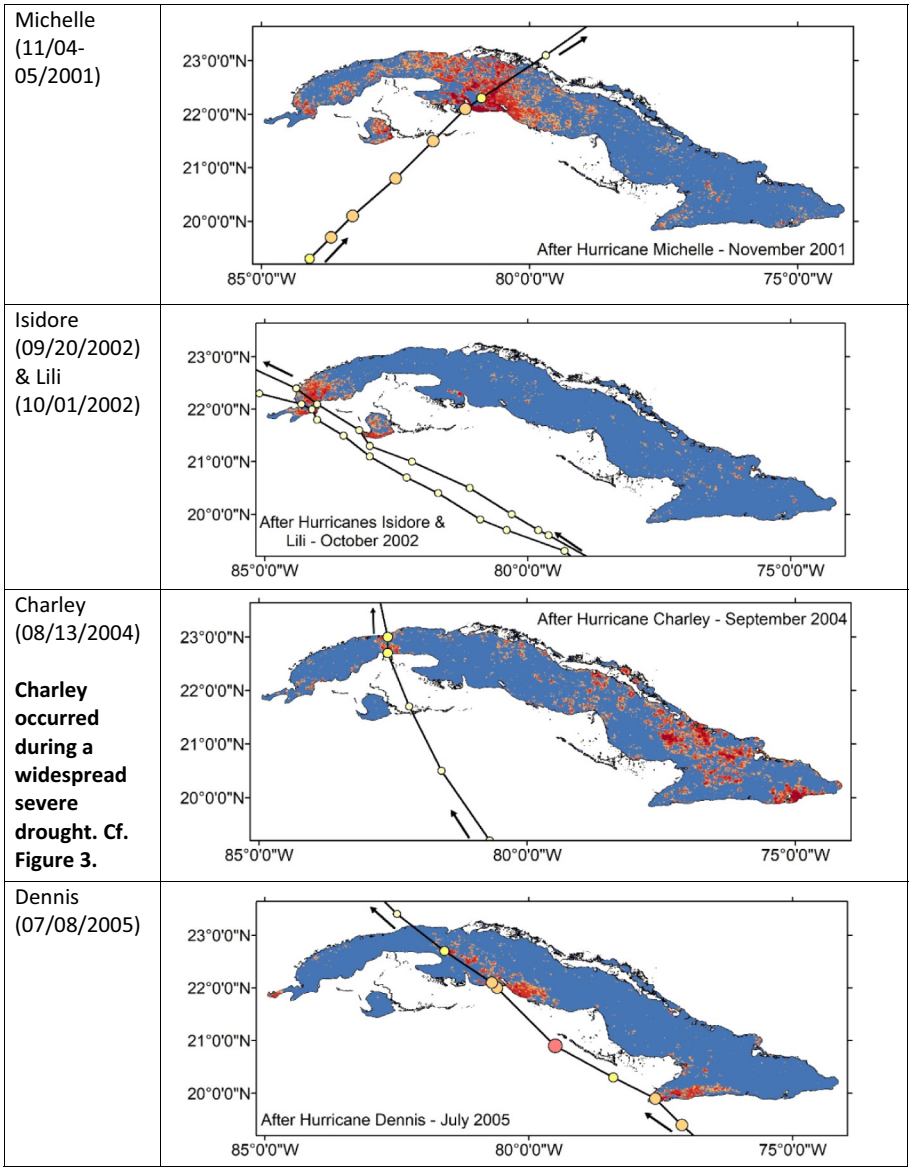

Fig. 5. Major hurricanes affecting Cuba and the observed disturbance data.

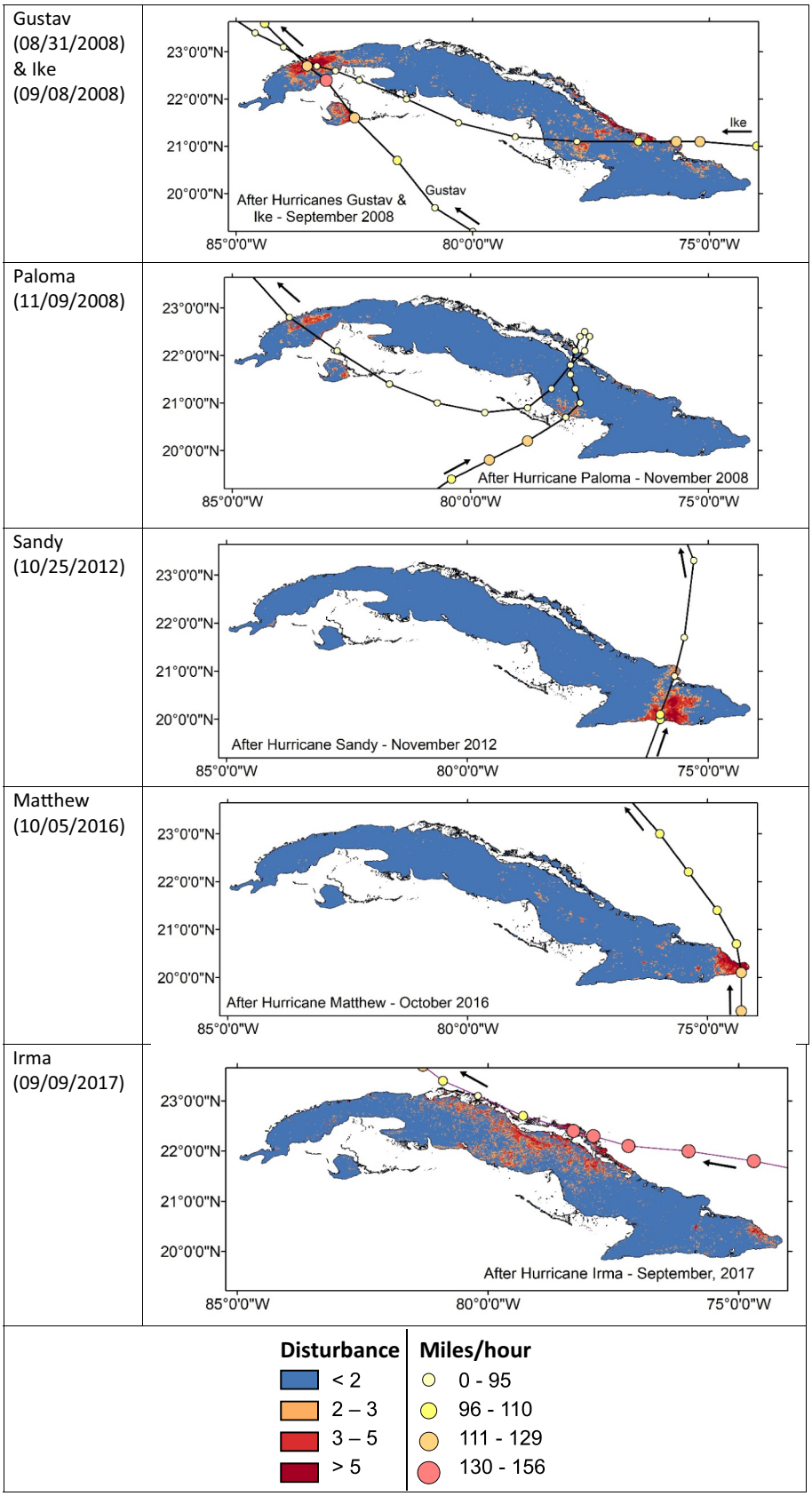

Fig. 5. (*continued*)

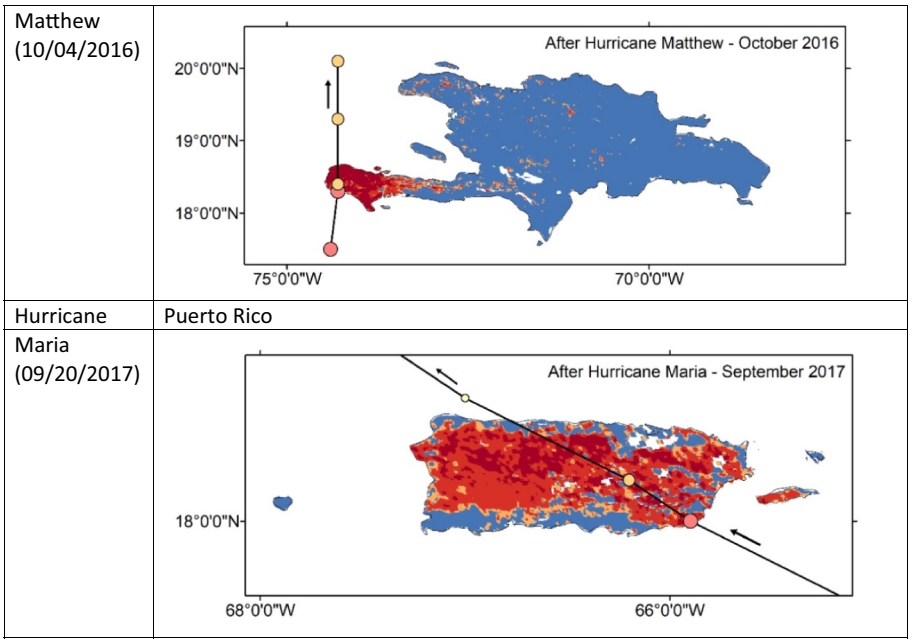

Fig. 6. Major hurricanes affecting Hispaniola and Puerto Rico, and the observed disturbance data. The legend for the hurricane speeds and the disturbance data can be found in Fig. 5.

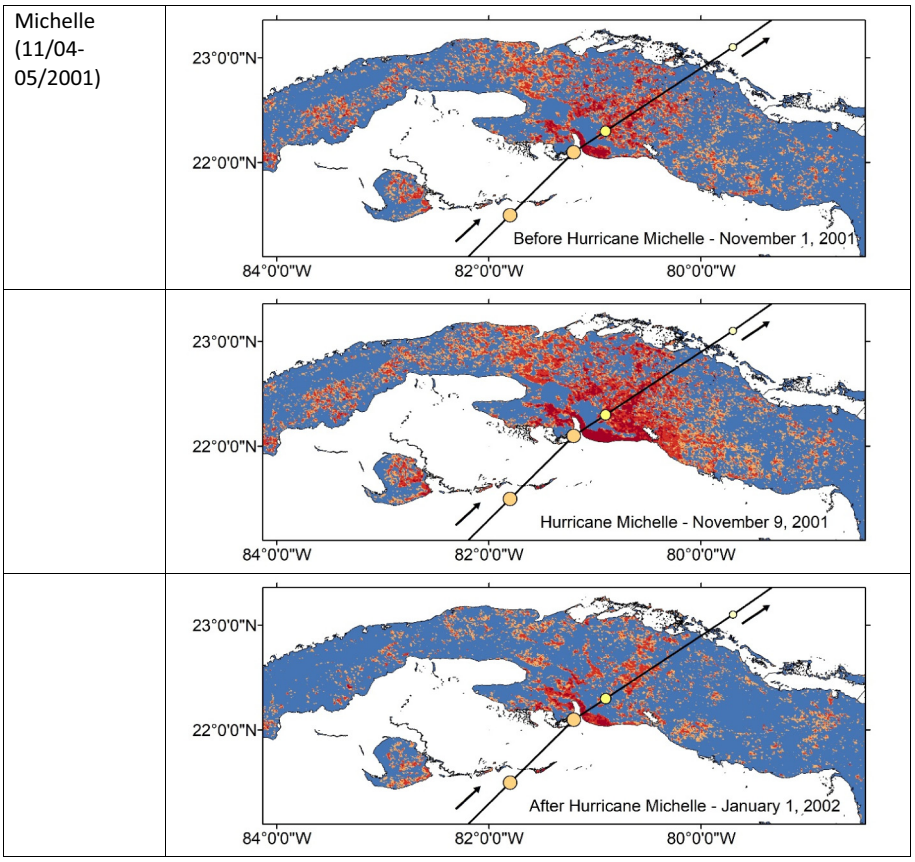

Fig. 7. Before hurricane Michelle (top), Cuba already displayed a relatively large amount of disturbance. This disturbance increased substantially immediately after hurricane Michele made landfall on Cuba (middle). About two months after the hurricane made landfall, the drought has been alleviated somewhat and some of the immediate disturbance has recovered (bottom). The legend for the hurricane speed and the disturbance data can be found in Fig. 5.

significantly disturbed (DI > 3). The percentage of disturbed area declined immediately when drought conditions eased. Similar responses are evident in Hispaniola after the 2003 drought, as well as in Puerto Rico (*e.g.*, 2015) and Jamaica (2004–2005 and 2013–2016), although the percentage of disturbed land on these islands rarely exceeded 25%. When we compare the PDSI with the DI spatially, we observe that there is greater variation in the DI data than in the PDSI data resulting from the difference in spatial resolution: approximately 4 km for the PDSI *versus* 500 m for the DI (Fig. 4). Note that the PDSI data provides a measurement of climatological drought severity, while the DI provides a measurement of the damage to the vegetation. Not every drought event will directly result in disturbance apparent in the landscape. For

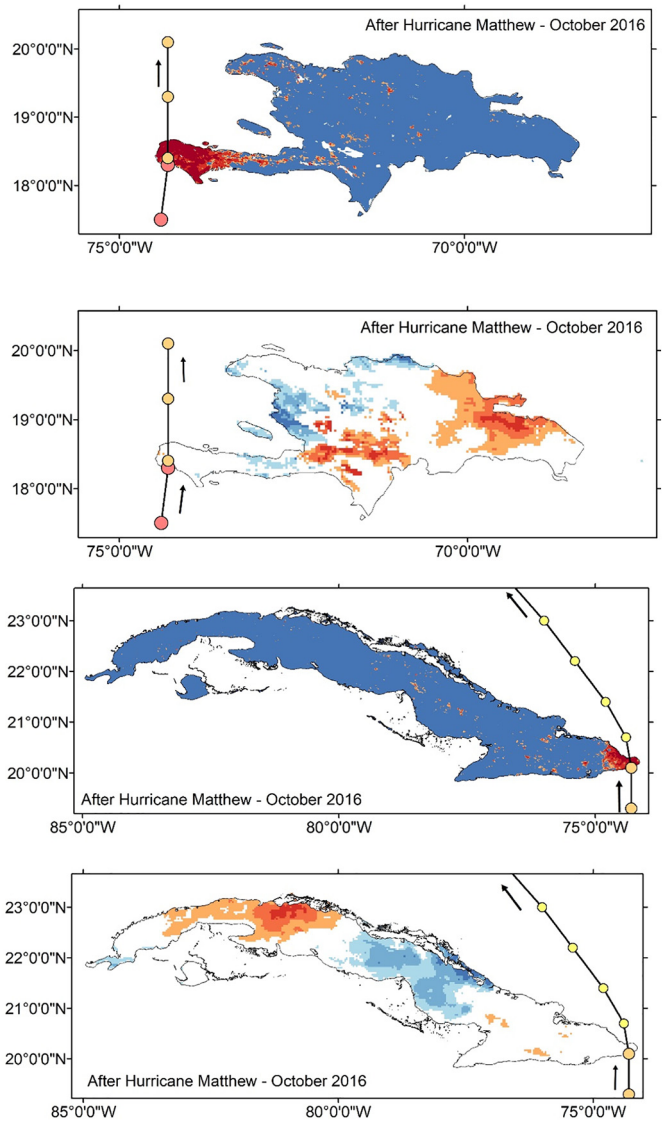

Fig. 8. Hurricane Matthew causing disturbance on Hispaniola and Cuba, but relieving drought. The legends for the PDSI and the disturbance data can be found in Fig. 4.

example, irrigation or urban landscapes might not experience any disturbance from the lack of precipitation because soil moisture is maintained through human intervention. In Puerto Rico, the severe drought of August 2015 did not affect the landscape evenly, with no significant disturbance in large parts of the central forested highlands (Fig. 4). A similar pattern is visible in Jamaica, where the drought that started in the beginning of 2015 and lasted through the end of the observation period (December 2016) is evident almost everywhere across the island, while the main area of disturbance is visible only in the central portion of the island.

5.3. Disturbance detection: hurricanes

The disturbance index can clearly reveal the impact of hurricanes. We have mapped out all hurricanes that hit Cuba between 2001 and 2016 (Fig. 5) as well as the impact of Matthew on Hispaniola and Maria on Puerto Rico (Fig. 6).

Isidor and Lili in 2002 were combined into one map, as were Gustav and Ike in 2008, because the hurricanes occurred within one month of each other, making the damage from their crossing paths difficult to separate. The impacts from each hurricane are clearly visible on the landscape, with greater windspeeds causing significantly more damage (Figs. 5, 6). We also find that while the effect of the hurricanes can be devastating, the total area affected is relatively localized, except for hurricane Maria, which affected all areas of Puerto Rico. The damage from Michelle and Charley on Cuba appears larger and more widespread than expected, as a result of concurrent drought (Fig. 3). Hurricane Michelle struck Cuba in the middle of a short but severe drought (Fig. 7). The widespread drought effect is clearly visible on Cuba's landscape right before the hurricane hit, but the disturbance index reveals increased disturbance in the area where Michelle hit. The drought is clearly alleviated following the rains delivered by Michelle (Fig. 7, bottom).

Fig. 8 also shows that the rainfall brought by hurricane Matthew alleviated drought conditions on Hispaniola and Cuba.

5.4. Disturbance validation

Hurricane damage detection is not necessarily straightforward, even when high resolution images are available. Fig. 9 reveals a damaged area in Puerto Rico after Hurricane Maria.

As mentioned earlier, cloud cover can make it difficult to find unobscured high-resolution imagery to map hurricane damage in the Caribbean. We selected before and after images for Hurricane Matthew in Hispaniola and Hurricane Maria in Puerto Rico to validate the disturbance data (Fig. 10). For Hurricane Matthew, we identified that 21 of the 25 samples visually revealed hurricane damage, two samples were too cloudy to identify any damage, and we were unable to identify damage on the remaining two sites (Fig. 10). We identified the disturbance index values both before the hurricane hit and three weeks after the hurricane event based on the MODIS data for the 21 samples for which we confirmed hurricane damage (Fig. 10). Before the hurricane, the disturbance index was not significantly different from zero, which is our expected value for no damage. After the hurricane the disturbance index was significantly higher, with an average DI value of 5.92, and 20 out of 21 samples revealed disturbance values well above zero.

We were able to identify a greater number of samples for Maria, which allowed us to separate the effect of hurricanes on developed lands from the impact on vegetated land (Fig. 10, Table 4). We found that the disturbance index was not significantly different from 0 before Maria hit Puerto Rico. After Maria hit the average disturbance index increased to 2.40 for developed land and 3.37 for vegetated land. Thus, the disturbance index was capable of measuring disturbance on both land covers, but the increase in the disturbance index was higher over vegetated land compared to developed land and, while the developed areas revealed an increase in DI, the ultimate DI values was often not above two after the hurricane (Table 3).

It is important to emphasize here that it is much easier to identify that a sample displayed damage, than to identify the absence of damage. As a result, we focused our validation efforts on the detection of damage. Nevertheless, we note that before the hurricane hit the average disturbance values were zero (the expected value for areas with no damage).

6. Discussion

6.1. Remotely sensed hurricane damage detection

A review of the literature results in several papers which rely, at least partly, on the use of vegetation indices, such as the Normalized Difference Vegetation Index (NDVI) or the Enhanced Vegetation Index (EVI) for the detection of hurricane damage. For example, before and after MODIS Enhanced Vegetation Index (EVI) imagery were used to detect damage of Hurricane Felix on the broadleaf and pine forests of Nicaragua (Rossi et al., 2013). They reported greater damage in the broadleaf forests, with > 75% of the trees blown down in some areas,

Fig. 9. Before and after damage detection for a mixed urban/vegetated area Puerto Rico. The MODIS based disturbance index had a value of 1.43, which increased to 2.98 after the storm. Green vegetation is visible on both images. However, the after image shows the disappearance of several trees in the urban area, as well as a browning of the forested region in the upper left. Note that the disturbance value before the storm was relatively high (1.43) as a result of the mixed nature of this pixel and a drought. Nevertheless, the disturbance index increased substantially as a result of the storm. (For interpretation of the references to colour in this figure legend, the reader is referred to the web version of this article.)

than in the pine forest. They concluded that the spatial resolution of the 250 m MODIS data was sufficient for damage assessments after hurricanes in (sub-)tropical forests. Two other studies investigating hurricane landfall damage along the northern Gulf of Mexico and southeastern Yucatan in Mexico also used differences in EVI to measure hurricane damage (Rogan et al., 2011; Wang and D'sa, 2009) with similar results. While it is possible to use NDVI or EVI to investigate hurricane damage (Hu and Smith, 2018), we have demonstrated previously that the defoliation and surface disturbance detected as a result of tornadoes disappears more quickly when analyzed with NDVI data than with disturbance index data (Kingfield and de Beurs, 2017). We have found a similar effect in this paper for the hurricane damage on the Caribbean islands; for example, Hu and Smith (2018) indicated that vegetation returned to near-normal about 1.5 months after Hurricane Maria affected Puerto Rico and Dominica in 2017. Recovery from disturbance appeared much slower when analyzed using our disturbance index approach. After Hurricane Maria hit Puerto Rico, we found that 50% of Puerto Rico (4549 km^2) showed significant disturbance (DI > 3). We found signs of recovery in the disturbance data starting about 8–12 weeks after hurricane Maria hit; however, by the end of 2017, the disturbance index was still > 3 across 31% of the island (2822 km^2).

We believe that the quick recovery in NDVI data is often the result of increased rainfall generating a leaf pulse in hurricane-affected vegetation (Parker et al., 2017). Although the remotely sensed data might reveal a return to normal levels of NDVI relatively quickly, the actual vegetation canopy can take much longer to recover to pre-disturbance conditions. For example, tall mangrove stands might take > 20 years to recover fully; whereas, shrublands can recover much more quickly (Imbert, 2018). In Taiwan, it took two years for litterfall to return to pre-typhoon levels after a major event in 1994, and annual peak leaf area index only returned to pre-event levels after ten years (Lin et al., 2017).

Instead of one of the more common vegetation indices, such as NDVI or EVI, a few studies have investigated changes in the leaf water content after hurricanes (Jin and Sader, 2005; Wang et al., 2010), for example using the Normalized Difference Infrared Index (NDII) that combines the near infrared (NIR) and shortwave infrared (SWIR) bands. Wang et al. (2010) indicated that NDII was more sensitive to vegetation changes after hurricanes, especially in areas dominated by forests, which results in loss of NDVI sensitivity due to higher levels of leaf area index (Vina et al., 2004). Others have also expanded to other parts of the electromagnetic spectrum. For example, a MODIS instantaneous Global Disturbance Index using EVI and Land Surface Temperature (LST) was developed to detect disturbances, such as hurricanes, across North America (Mildrexler et al., 2009). An evaluation of the effects of Hurricanes Katrina, Rita, and Wilma revealed that this disturbance index was able to pick up the expected effect of high severity disturbance near the shoreline and moderate severity disturbance inland, although the authors acknowledged that more research was necessary to evaluate the moderate severity disturbance detections.

Wang and Xu (2010) compared four different algorithms and several different spectral indices to assess the damage of Hurricane Katrina on forests. They found that the impact of the selection of classification method was less important than the effect of the selection of the spectral index. They also found that the Tasseled Cap Wetness index outperformed five other tested indices and that a post-classification comparison proved the most accurate methodology (Wang and Xu, 2010). (See Wang et al. (2010) for an overview of other post-storm damage assessment studies, predominantly using vegetation indices.)

6.2. Hurricane and drought interaction

Vegetation gains due to additional rainfall are regularly observed in the aftermath of hurricanes. For example, in dryland forests, where an increase in the NDVI was visible within a few months after Hurricanes Jova and Patricia affected Mexico (Parker et al., 2017). We have demonstrated that the MODIS disturbance index standardized in time is effective at identifying disturbance resulting from both hurricanes and droughts. An example of drought and hurricane interaction can be found after Hurricane Matthew (Fig. 8). It was the strongest storm to impact Haiti (western Hispaniola) since the early 1960s, resulting in major damage and as many as 546 deaths. Hurricane Matthew hit both Cuba and Hispaniola as a category 4 hurricane, depositing between 400 mm and 500 mm of rain in these countries and effectively alleviating a drought in parts of these islands (Fig. 8). This impact is not unlike the effect of Atlantic tropical cyclones on drought over the Eastern United States (Kam et al., 2013; Maxwell et al., 2013). We have also demonstrated that not every climatological drought condition results in an observable disturbance to the landscape, with drought effects being often slow to appear in forested areas (*e.g.*, Fig. 4).

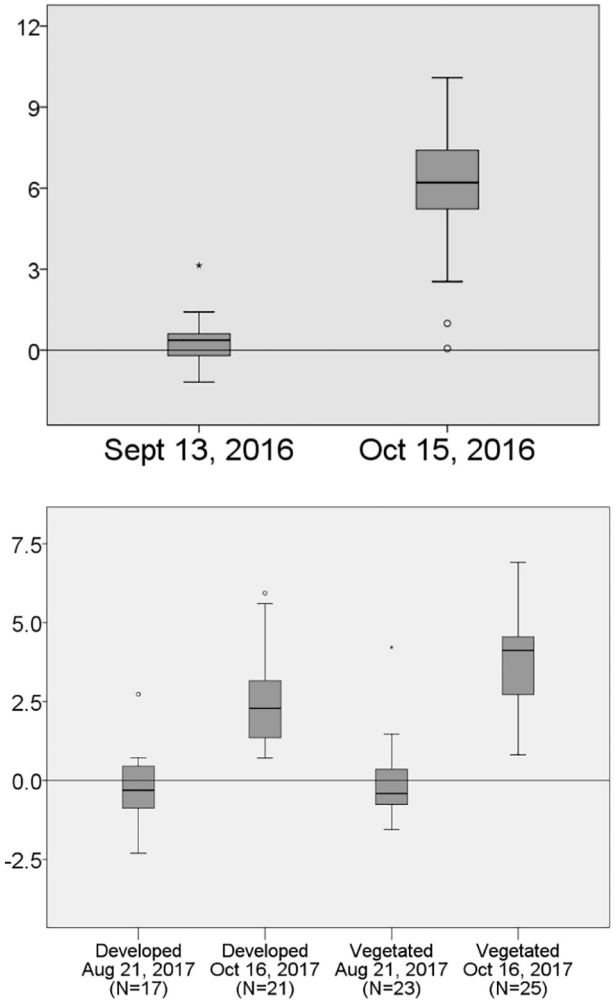

Fig. 10. (top): Boxplot shows the distribution of the mean DI for all validation points showing visually identified hurricane damage one week before Hurricane Matthew and three weeks after the hurricane. ($N = 21$). (bottom): Box plot showing the distribution of the mean DI of validation points on Puerto Rico when sorted between developed (urban and suburban) and vegetated (forest, scrub, and other natural vegetation). Not that the y-axes are different for the two sets to better visualize the distributions.

Table 4
Number of samples that are visibly damaged and their corresponding DI class according to MODIS.

	Developed	Vegetated	Total
MODIS DI < 2	14	4	18
MODIS DI > 2	7	21	28
Total	21	25	46

6.3. Validation of hurricane damage

While the MODIS-derived disturbance index can be used to track damage and recovery from both hurricanes and droughts on vegetated and developed lands, we have found that it is more sensitive to disturbances on vegetated landscapes. This sensitivity is a result of the incorporation of the Tasseled Cap greenness index, which measures declines in greenness on the landscape and the exposure of soils after disturbances. It is also important to point out that large-scale validation of the effect of hurricanes is complicated in several ways:

1) Hurricane damage significantly hampers field validation opportunities, and it is difficult to plan large field campaigns around the potential for hurricanes. As a result, it is very difficult to tie the disturbance index values to ground damage assessments.
2) Hurricane damage often occurs during periods and in regions with very dense cloud cover. As a result, it is difficult to find high resolution, or even moderate resolution cloud-free before and after satellite images as we experienced in this study. As an example, we have downloaded all Landsat images (L1T) from 1984 until now during the hurricane season (July–December) for two Landsat WRS-2 Path/Row scenes (P16/R44 and P11/R46) in the East and West of Cuba. Over the entire time period we found a total of 301 images in Western Cuba, and 361 images in Eastern Cuba. For each image we used the provided quality assessment data to identify if a pixel contains cloud cover. Fig. 11 provides a cloud climatology based on these Landsat footprints over Cuba showing that almost half (48.31%) of P11//R46 was cloud-free < 50% of the time and 70% of P16/R44 was cloud-free < 50% of the time. In addition, coastal areas, where the hurricane damage is often the most severe, show even higher percentages of clouds, some regions missing as much as 80% of the data. This cloud climatology also explains why it is so difficult to carry out standardized "before-and-after" comparisons to identify hurricane damage, *e.g.*, the probability of finding a cloud-free before-and-after pixel pair can be calculated by multiplying the values in Fig. 11. Lastly, expanding the potential "before" and "after" time periods for comparison, might aid in the probability of finding cloud-free data, but as described above, hurricane damage can recover rather quickly. Thus, the potential for finding a standardized hurricane response will be greatly diminished.
   For comparison purposes, we also investigated New Orleans (P22/R39) and Oklahoma City (P28/R35). We found significantly more images for New Orleans (496), but determined that 50% of the area was cloud-free < 50% of the time, similar to Cuba. In contrast, Oklahoma City, which is more inland, showed that the 50% of the pixels were cloud-free at least 80% of the time.
3) While we note that droughts are visible in the disturbance index data, we did not provide an explicit validation of the effect of droughts (other than Fig. 3). We also did not attempt to use the disturbance index data to identify whether a disturbance is the result of drought, or the result of hurricane damage. Since we had good hurricane track data available (Hurdat 2), we assumed that disturbances detected immediately after a hurricane are due to that event. *Vice versa*, since we had good drought data available (Herrera and Ault, 2017), we assumed that disturbance identified to coincide with observed droughts are due to that hazard. Instead, we proposed this standardized dataset approach as a way to identify the damage caused by these two natural hazards in a standardized manner that enables comparison of the effects of hurricanes over time and for different ecosystems.

6.4. Other available data sources

Hurricanes often cause significant flooding in addition to major wind damage. It is not possible to use the MODIS disturbance data to map the flooding as it is ongoing, because the optical MODIS sensor is unable to penetrate the significant cloud cover that accompanies hurricanes. A recent paper demonstrates the use of Cyclone Global Navigation Satellite Systems (CYGNSS) data, which has a spatial resolution of a few kilometers and a temporal resolution of just a few days (Chew et al., 2018). Combining these types of data with the MODIS disturbance index might generate an opportunity to better understand where flooding occurs and how long the damage remains visible on the landscape. Visual evaluations reveal very similar damage agreements between the CYGNSS data and the MODIS disturbance data reported here for Hurricane Irma.

The Visible Infrared Imaging Radiometer Suite (VIIRS) flying on the

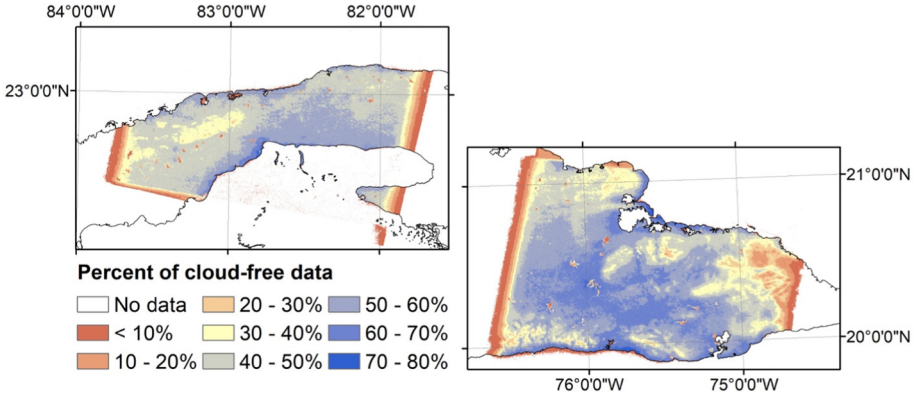

Fig. 11. Cloud climatology for Landsat WRS-2 P16/R44 and P11/R46 over Cuba.

Suomi National Polar-orbiting Partnership (NPP) satellite since 2011 is the operational replacement for the MODIS sensors that are currently in service well beyond their six-year life span. To transfer the disturbance index methodology presented here to the VIIRS data, it will be crucial to understand how the VIIRS data with a much shorter temporal record can be standardized against the MODIS observed time series. The VIIRS spectral bands are slightly different than the MODIS bands. Tasseled Cap coefficients will need to be newly developed for VIIRS, and we are not aware that any such coefficients have yet been developed.

It is important to point out that our disturbance dataset is unable to estimate monetary damages: economic impacts on developed land are usually much greater than the impacts on vegetated areas. While the spectral bands available on VIIRS are comparable to the MODIS bands, VIIRS also has a Day/Night Band, which is particularly sensitive to very low levels of light and allows for the tracking of nighttime lights. These data have been used to understand the effect of hurricanes on power outages that can be directly linked to the socio-economic impact of these storms (Cao et al., 2013; Miller et al., 2018). Another potential opportunity for the use of the VIIRS data would be to link our disturbance dataset with data from the VIIRS day/night band (Román et al., 2018), which might prove useful for the understanding of damage on both vegetated and developed land surfaces (Wang et al., 2018).

7. Conclusions

To better study the combined effects from droughts and hurricanes, it is important to have a stable disturbance dataset that (1) is not strongly influenced by seasonal variation and (2) can be used to track recovery from hurricanes in a standardized way. Based on this dataset, it will be possible to evaluate whether the size of the damage area from hurricanes can be predicted based on the hurricane strength, whether there is a seasonal difference in damage severity and recovery time, or whether certain ecosystems recover more rapidly than others. Furthermore, it will be possible to start teasing apart the effects of droughts and hurricanes. For example, do hurricanes cause damage in larger areas if preceded by a drought? Is the damage more severe after drought (*e.g.*, higher disturbance index values) or does it take longer for the ecosystem to recover? The disturbance index approach developed in this paper can be used in such a manner to not only report the damage from one or a few hurricanes, but to report the damage of multiple hurricanes in a standardized fashion. The dataset is also capable of identifying the damage from both droughts and hurricanes, which can be used to better understand how the combined effects of these two natural hazards impact landscapes.

Acknowledgements

This research was supported in part by the NASA Science of Terra & Aqua project NNX14AJ32G entitled *Change in our MIDST: Detection and analysis of land surface dynamics in North and South America using multiple sensor datastreams.* The authors thank Prof. Toby Ault of Cornell University for the use of his dataset. The MCD43A4 product was retrieved from the data pool of the NASA EOSDIS Land Processes Distributed Active Archive Center (LP DAAC), USGS/Earth Resources Observation and Science (EROS) Center, Sioux Falls, South Dakota. The authors thank the helpful input of two anonymous reviewers that helped improve the clarity of the presentation.

References

Atlantic Hurdat2, 2018. Atlantic HURDAT2. pp Page. https://www.nhc.noaa.gov/data/hurdat/hurdat2-format-atlantic.pdf.
Beard, K.H., Vogt, K.A., Vogt, D.J., et al., 2005. Structural and functional responses of a subtropical forest to 10 years of hurricanes and droughts. Ecol. Monogr. 75, 345–361.
Cao, C., Shao, X., Uprety, S., 2013. Detecting light outages after severe storms using the S-NPP/VIIRS day/night band radiances. IEEE Geosci. Remote Sens. Lett. 10, 1582–1586.
Chambers, J.Q., Fisher, J.I., Zeng, H., Chapman, E.L., Baker, D.B., Hurtt, G.C., 2007. Hurricane Katrina's carbon footprint on US Gulf Coast forests. Science 318, 1107.
Chew, C., Reager, J.T., Small, E., 2018. CYGNSS data map flood inundation during the 2017 Atlantic hurricane season. Scientific Reports (Nature Publisher Group) 8, 1–8.
Curtis, S., 2008. The Atlantic multidecadal oscillation and extreme daily precipitation over the US and Mexico during the hurricane season. Clim. Dyn. 30, 343–351.
de Beurs, K.M., Owsley, B.C., Julian, J.P., 2016. Disturbance analyses of forests and grasslands with MODIS and Landsat in New Zealand. Int. J. Appl. Earth Obs. Geoinf. 45, 42–54.
Elder, R.C., Balling Jr., R.C., Cerveny, R.S., Krahenbuhl, D., 2014. Regional variability in drought as a function of the Atlantic Multidecadal Oscillation. Caribb. J. Sci. 48, 31–43.
Emanuel, K., 2005. Increasing destructiveness of tropical cyclones over the past 30 years. Nature 436, 686.
Faust, E., Bove, M., 2017. In: Re, M. (Ed.), The Hurricane Seasons 2017: A Cluster of Extreme Storms, pp Page. https://www.munichre.com/topics-online/en/2017/12/hurricane-season-2017#experts (Munich RE).
Fensterer, C., Scholz, D., Hoffmann, D., Spötl, C., Pajón, J.M., Mangini, A., 2012. Cuban stalagmite suggests relationship between Caribbean precipitation and the Atlantic Multidecadal Oscillation during the past 1.3 ka. The Holocene 22, 1405–1412.
Gómez, C., White, J.C., Wulder, M.A., 2016. Optical remotely sensed time series data for land cover classification: a review. ISPRS J. Photogramm. Remote Sens. 116, 55–72.
Healey, S.P., Cohen, W.B., Zhiqiang, Y., Krankina, O.N., 2005. Comparison of Tasseled Cap-based Landsat data structures for use in forest disturbance detection. Remote Sens. Environ. 97, 301–310.
Herold, M., Mayaux, P., Woodcock, C., Baccini, A., Schmullius, C., 2008. Some challenges in global land cover mapping: an assessment of agreement and accuracy in existing 1 km datasets. Remote Sens. Environ. 112, 2538–2556.
Herrera, D., Ault, T., 2017. Insights from a new high-resolution drought Atlas for the Caribbean spanning 1950–2016. J. Clim. 30, 7801–7825.
Hu, T., Smith, R.B., 2018. The impact of hurricane Maria on the vegetation of Dominica and Puerto Rico using multispectral remote sensing. Remote Sens. 10, 827.
Imbert, D., 2018. Hurricane disturbance and forest dynamics in east Caribbean mangroves. Ecosphere 9, e02231.
Jin, S., Sader, S.A., 2005. Comparison of time series tasseled cap wetness and the normalized difference moisture index in detecting forest disturbances. Remote Sens. Environ. 94, 364–372.
Kam, J., Sheffield, J., Yuan, X., Wood, E.F., 2013. The influence of Atlantic tropical cyclones on drought over the eastern United States (1980–2007). J. Clim. 26, 3067–3086.
Kingfield, D.M., de Beurs, K.M., 2017. Landsat identification of tornado damage by land cover and an evaluation of damage recovery in forests. J. Appl. Meteorol. Climatol.

56, 965–987.
Knutson, T.R., Mcbride, J.L., Chan, J., et al., 2010. Tropical cyclones and climate change. Nat. Geosci. 3, 157.
Landsea, C.W., Franklin, J.L., 2013. Atlantic hurricane database uncertainty and presentation of a new database format. Mon. Weather Rev. 141, 3576–3592.
Lin, K.-C., Hamburg, S.P., Wang, L., Duh, C.-T., Huang, C.-M., Chang, C.-T., Lin, T.-C., 2017. Impacts of increasing typhoons on the structure and function of a subtropical forest: reflections of a changing climate. Sci. Rep. 7, 4911.
Lobser, S., Cohen, W., 2007. MODIS tasselled cap: land cover characteristics expressed through transformed MODIS data. Int. J. Remote Sens. 28, 5079–5101.
Long, J., Giri, C., Primavera, J., Trivedi, M., 2016. Damage and recovery assessment of the Philippines' mangroves following Super Typhoon Haiyan. Mar. Pollut. Bull. 109, 734–743.
Lugo, A.E., 2000. Effects and outcomes of Caribbean hurricanes in a climate change scenario. Sci. Total Environ. 262, 243–251.
Maxwell, J.T., Ortegren, J.T., Knapp, P.A., Soulé, P.T., 2013. Tropical cyclones and drought amelioration in the Gulf and southeastern coastal United States. J. Clim. 26, 8440–8452.
Méndez, M., Magaña, V., 2010. Regional aspects of prolonged meteorological droughts over Mexico and Central America. J. Clim. 23, 1175–1188.
Mildrexler, D.J., Zhao, M., Running, S.W., 2009. Testing a MODIS global disturbance index across North America. Remote Sens. Environ. 113, 2103–2117.
Miller, S.D., Straka Iii, W.C., Yue, J., et al., 2018. The dark side of hurricane Matthew: unique perspectives from the VIIRS day/night band. Bull. Am. Meteorol. Soc. 99, 2561–2574.
Negrón-Juárez, R., Baker, D.B., Chambers, J.Q., Hurtt, G.C., Goosem, S., 2014. Multi-scale sensitivity of Landsat and MODIS to forest disturbance associated with tropical cyclones. Remote Sens. Environ. 140, 679–689.
Ortegren, J.T., Maxwell, J.T., 2014. Spatiotemporal patterns of drought/tropical cyclone co-occurrence in the Southeastern USA: linkages to North Atlantic climate variability. Geogr. Compass 8, 540–559.
Parker, G., Martínez-Yrízar, A., Álvarez-Yépiz, J.C., Maass, M., Araiza, S., 2017. Effects of hurricane disturbance on a tropical dry forest canopy in western Mexico. For. Ecol. Manag. 426, 39–52.
Pielke Jr., R.A., Landsea, C., Mayfield, M., Layer, J., Pasch, R., 2005. Hurricanes and global warming. Bull. Am. Meteorol. Soc. 86, 1571–1576.
Potter, C., 2014. Global assessment of damage to coastal ecosystem vegetation from tropical storms. Remote Sensing Letters 5, 315–322.
Rogan, J., Schneider, L., Christman, Z., Millones, M., Lawrence, D., Schmook, B., 2011. Hurricane disturbance mapping using MODIS EVI data in the southeastern Yucatán, Mexico. Remote Sensing Letters 2, 259–267.
Román, M.O., Wang, Z., Sun, Q., Kalb, V., Miller, S.D., Molthan, A., Schultz, L., Bell, J., Stokes, E.C., Pandey, B., Seto, K.C., 2018. NASA's Black Marble nighttime lights product suite. Remote Sens. Environ. 210, 113–143.
Rossi, E., Rogan, J., Schneider, L., 2013. Mapping forest damage in northern Nicaragua after hurricane Felix (2007) using MODIS enhanced vegetation index data. GIScience & remote sensing 50, 385–399.
Schaaf, C.B., Gao, F., Strahler, A.H., et al., 2002. First operational BRDF, albedo nadir reflectance products from MODIS. Remote Sens. Environ. 83, 135–148.
Steinskog, D.J., Tjøstheim, D.B., Kvamstø, N.G., 2007. A cautionary note on the use of the Kolmogorov–Smirnov test for normality. Mon. Weather Rev. 135, 1151–1157.
Tran, T.V., de Beurs, K.M., Julian, J.P., 2016. Monitoring forest disturbances in Southeast Oklahoma using Landsat and MODIS images. Int. J. Appl. Earth Obs. Geoinf. 44, 42–52.
Trenberth, K.E., Dai, A., Van Der Schrier, G., Jones, P.D., Barichivich, J., Briffa, K.R., Sheffield, J., 2014. Global warming and changes in drought. Nat. Clim. Chang. 4, 17.
Vina, A., Henebry, G.M., Gitelson, A.A., 2004. Satellite monitoring of vegetation dynamics: sensitivity enhancement by the wide dynamic range vegetation index. Geophys. Res. Lett. 31.
Wang, F., D'sa, E.J., 2009. Potential of MODIS EVI in identifying hurricane disturbance to coastal vegetation in the northern Gulf of Mexico. Remote Sens. 2, 1–18.
Wang, F., Xu, Y.J., 2010. Comparison of remote sensing change detection techniques for assessing hurricane damage to forests. Environ. Monit. Assess. 162, 311–326.
Wang, W., Qu, J.J., Hao, X., Liu, Y., Stanturf, J.A., 2010. Post-hurricane forest damage assessment using satellite remote sensing. Agric. For. Meteorol. 150, 122–132.
Wang, Z., Román, M.O., Sun, Q., Molthan, A.L., Schultz, L.A., Kalb, V.L., 2018. Monitoring disaster-related power outages using NASA black marble nighttime light product. Int. Arch. Photogramm. Remote. Sens. Spat. Inf. Sci. 1853–1856.
World Bank, 2018. World Development Indicators. pp Page. https://data.worldbank.org/indicator/The World Bank.
Xuan, Z., Chang, N.-B., 2014. Modeling the climate-induced changes of lake ecosystem structure under the cascade impacts of hurricanes and droughts. Ecol. Model. 288, 79–93.